Polymer 49 (2008) 3568–3577

Contents lists available at ScienceDirect

Polymer

journal homepage: www.elsevier.com/locate/polymer

Dispersion of polymer-grafted magnetic nanoparticles in homopolymers and block copolymers

Chen Xu [a], Kohji Ohno [b], Vincent Ladmiral [b,1], Russell J. Composto [a,*]

[a] Department of Materials Science and Engineering and Laboratory for Research on the Structure of Matter, University of Pennsylvania, Philadelphia, PA 19104-6272, USA
[b] Institute for Chemical Research, Kyoto University, Uji, Kyoto 611-0011, Japan

ARTICLE INFO

Article history:
Received 9 March 2008
Received in revised form 25 May 2008
Accepted 30 May 2008
Available online 4 June 2008

Keywords:
Polymer-grafted nanoparticles
Polymer nanocomposites
Nanoparticle dispersion

ABSTRACT

The dispersion of magnetic nanoparticles (NPs) in homopolymer poly(methyl methacrylate) (PMMA) and block copolymer poly(styrene-*b*-methyl methacrylate) (PS-*b*-PMMA) films is investigated by TEM and AFM. The magnetite (Fe_3O_4) NPs are grafted with PMMA brushes with molecular weights from $M = 2.7$ to 35.7 kg/mol. Whereas a uniform dispersion of NPs with the longest brush is obtained in a PMMA matrix ($P = 37$ and 77 kg/mol), NPs with shorter brushes are found to aggregate. This behavior is attributed to wet and dry brush theory, respectively. Upon mixing NPs with the shortest brush in PS-*b*-PMMA, as-cast and annealed films show a uniform dispersion at 1 wt%. However, at 10 wt%, PS-*b*-PMMA remains disordered upon annealing and the NPs aggregate into 22 nm domains, which is greater than the domain size of the PMMA lamellae, 18 nm. For the longest brush length, the NPs aggregate into domains that are much larger than the lamellae and are encapsulated by PS-*b*-PMMA which form an onion-ring morphology. Using a multi-component Flory–Huggins theory, the concentrations at which the NPs are expected to phase separate in solution are calculated and found to be in good agreement with experimental observations of aggregation.

1. Introduction

Inorganic nanoparticles (NPs) have been the subject of intense research over the past decade because of their potential as electronic, photonic, magnetic, and biomedical materials [1–6]. Incorporation of these NPs into polymer matrices results in polymer nanocomposites (PNC), which combine the functionality of the NPs with the processability of the matrix [7–13]. Typically, the dispersion of NPs in polymer matrices is problematic and the NPs tend to macrophase separate or aggregate in the host matrix [14]. However, a dispersion of NPs in the matrix is necessary to fully utilize the NP properties to achieve optimal performance of the device. In the absence of repulsive interactions, van der Waals attraction between NPs favors clustering and aggregation. NPs can be prevented from aggregating by grafting polymer brushes or adsorbing surfactant molecules to their surfaces. The most common approach to prepare PNC is to mix preformed NPs into a polymer matrix. Surface modification of the preformed NPs is usually required to achieve good dispersion in polymer matrices. Traditionally, coupling agents or surfactants have been widely used to stabilize the NPs [15,16]. More recently, "grafting to" and "grafting from" techniques have become popular methods to modify NPs with polymer brushes [17–26].

Choosing the proper polymer brush type and length will determine whether the modified NP will be favored, thermodynamically, to disperse in a polymer matrix. Typically, the brush has the same chemical composition as the homopolymer matrix or, in the case of block copolymers, one of the blocks [10,11,27,28]. A greater compatibility can be achieved by grafting brushes that have a favorable interaction (i.e., negative Flory–Huggins interaction parameter) with the polymer matrix. However, chemical matching is not the only factor controlling the compatibility of the polymer-grafted NPs in the polymer matrix [29]. The dispersion of polymer-grafted NPs in a homopolymer matrix also depends on other parameters including the molecular weight of polymer brush (M), the molecular weight of the matrix (P), and the grafting density of the brush [30–38]. For example, if the polymer brush is swollen or wet by the matrix chains, dispersion of the NPs will be favored [10,39,40]. For planar surfaces, dense polymer brushes are not wet by the matrix chains if $M < P$. The interaction between polymer-grafted spherical particles in a polymer melt has been studied theoretically by many research groups [29,41–47]. For example, Leibler and Borukhov used the self-consistent field (SCF) approach to predict the phase diagram for polymer-grafted NPs in a chemically identical polymer melt [29]. However, their theory is limited to colloidal particles where the radius is much larger than the polymer brush thickness.

* Corresponding author. Tel.: +1 215 898 4451; fax: +1 215 573 2128.
E-mail address: composto@seas.upenn.edu (R.J. Composto).
[1] Present address: Key Center for Polymer Colloids, School of Chemistry, University of Sydney, NSW 2006, Australia.

0032-3861/$ – see front matter © 2008 Elsevier Ltd. All rights reserved.
doi:10.1016/j.polymer.2008.05.040

Although many theoretical and experimental studies explore NPs in homopolymers, less attention has been paid to the dispersion of polymer-grafted NPs in block copolymers. In comparison to the homopolymer case, block copolymers introduce additional complexities due to new interactions and confinement effects [48]. For example, for the dispersion of polymer A-grafted NPs in an A–B copolymer, one has to consider the unfavorable interaction between brush A and block B. Recently, Lan et al. have investigated the dispersion of polystyrene-grafted silica NPs in homopolymer polystyrene (PS) and lamellar-forming poly(styrene-*b*-butadiene) (PS-*b*-PB) [49]. They found that NPs disperse for $M > P$ of the PS matrix, whereas an opposite trend was observed for the same NPs mixed with PS-*b*-PB, namely, NPs aggregate in PS-*b*-PB as M increases.

In the present study, we describe the dispersion of poly(methyl methacrylate) (PMMA)-grafted magnetite (Fe_3O_4) NPs in both a homopolymer, PMMA, and a block copolymer, poly(styrene-*b*-methyl methacrylate) (PS-*b*-PMMA). The magnetite NPs are grafted with PMMA brushes ranging from $M = 2.7$ to 35.7 kg/mol. The effect of M on the dispersion of NPs in PMMA and PS-*b*-PMMA is quite different. Namely, for a PMMA matrix with $P = 37$ ($\geq M$) or 77 kg/mol ($> M$), all NPs are found to uniformly disperse in as-cast films. Upon annealing, the NPs with the longest PMMA brush remains dispersed in PMMA, whereas NPs with $M = 2.7$ and 13.3 kg/mol tend to form aggregates whose size depends on the NP concentration. This behavior is consistent with the wet and dry brush theory which suggests that high M brushes are more easily wet by lower P matrices. However, upon mixing the PMMA-grafted NPs with PS-*b*-PMMA an opposite trend is observed. In the as-cast films, uniform dispersion is obtained for NPs with the shortest PMMA brush, whereas NPs aggregate as M increases. This experimental observation can be well described by a three-component Flory–Huggins theory that correctly predicts phase separation in the solution prior to casting.

2. Experimental section

2.1. Materials and methods

Poly(methyl methacrylate) (PMMA) homopolymers with molecular weights (P) of 37 and 77 kg/mol were purchased from Polymer Source, Inc. The polydispersities are 1.04 and 1.07, respectively. These homopolymers are denoted as PMMA-37K and PMMA-77K, respectively. The poly(styrene-*b*-methyl methacrylate) (PS-*b*-PMMA) with a polydispersity of 1.08 was purchased from Polymer Source, Inc. The molecular weights of the PS and PMMA blocks are 38 and 36.8 kg/mol, and the volume fractions of the blocks are $f_{PS} = 0.53$ and $f_{PMMA} = 0.47$, respectively. The PMMA-grafted magnetite (Fe_3O_4) NPs were prepared by grafting PMMA chains onto presynthesized magnetite NPs via surface-initiated atom transfer radical polymerization (ATRP) [24]. The magnetite NPs were synthesized and characterized following the methods described by Sun and Zeng [50]. To determine the molecular weight and polydispersity of the grafted polymer brush, PMMA chains were cleaved from the NP surface as follows: the PMMA-grafted magnetite NPs and tetraoctylammonium bromide as a phase transfer catalyst were dissolved in toluene, to which a 10% HF aqueous solution was added. The cleaved polymer in the organic layer was isolated, and then subjected to gel permeation chromatography (GPC) measurements. Three PMMA brushes with molecular weights (M_n) of 2.7, 13.3 and 35.7 kg/mol were employed in this study, and therefore the PMMA-grafted magnetite NPs are denoted as Fe_3O_4-2.7K, Fe_3O_4-13.3K and Fe_3O_4-35.7K, respectively. The polydispersity indexes of these PMMA brushes determined by GPC are 1.22, 1.10 and 1.15, respectively. The grafting density (Σ) was calculated to be $\sim$0.73 chains/nm^2 for all three NPs based on the weight fraction of PMMA chains (determined by thermal gravimetric analysis), the NP diameter, and densities of PMMA and magnetite. Thus, the total number of PMMA brushes per NP is about 60.

To prepare the polymer–nanoparticle nanocomposites, a 7 wt% polymer–nanoparticle solution in toluene is prepared. The weight fraction of NPs in the mixture of polymer and NPs ranges from 1 to 16 wt%. Nanocomposite films were prepared by spin casting this solution onto piranha cleaned silicon substrates. The films were dried in a vacuum oven at room temperature for 1 day, and the resulting nanocomposite films were about 500 nm thick. The films were then annealed under vacuum at 185 °C for different times.

2.2. Characterization

The NP core diameter was determined using transmission electron microscopy (TEM, JEOL 2010) operated at 80 kV. A monolayer of magnetite NPs was prepared by delivering a drop of dilute nanoparticle–toluene solution onto holy carbon coated copper grids (mesh size 300, Structure Probe, Inc). The NP core diameter distribution was obtained from TEM images of at least 150 particles using the grain analysis module from SPIP software (Image Metrology, Inc). The PMMA brush thickness (h) was estimated from the distance between adjacent particles in the monolayer film.

The surface morphology of the nanocomposite films was obtained using an atomic force microscope (AFM, PicoPlus, Agilent Technologies) in the acoustic AC (AAC) mode. Silicon cantilevers (PPP-NCL, Nanosensors) with a nominal spring constant of 48 N/m and tip radius of less than 10 nm were used. The resonance frequency of the PPP-NCL cantilevers is about 190 kHz. Picoscan 5.3.3 (Agilent Technologies) and SPIP were used for AFM image analysis. TEM was performed to characterize the structure of the nanocomposite films. To prepare TEM cross-sections, nanocomposite films were coated with an epoxy layer, and then immersed into liquid N_2 to delaminate the bi-layers of epoxy/nanocomposite film from the silicon substrates. The epoxy-supported nanocomposite films were microtomed into $\sim$50 nm slices with a diamond knife at room temperature. The microtomed sections were transferred onto holy carbon coated copper grids. Many cross-sectional TEM images were captured over different areas and the images shown in Section 3 are representative examples. The equivalent diameter of NP aggregates was determined by analyzing many TEM images using the SPIP software.

3. Results and discussion

3.1. PMMA-grafted magnetite nanoparticles

Fig. 1 shows TEM images of films containing only PMMA-grafted magnetite NPs deposited from a good solvent on a substrate. Fig. 1a–c represents NPs having brush molecular weights of $M = 2.7$, 13.3 and 35.7 kg/mol, respectively. The histograms below each image represent the corresponding diameters of the core particle, Fe_3O_4. For the statistical average denoted by the histograms, the core diameters are 5.4 ± 1.1, 5.4 ± 1.4 and 5.1 ± 1.3 nm, respectively. As shown in Fig. 1a–c, the separation between NPs increases as the brush length, or M, increases. The PMMA brush thickness (h) corresponding to the deposition conditions can be determined from the distance between adjacent particles. For Fe_3O_4-2.7K, Fe_3O_4-13.3K and Fe_3O_4-35.7K, the average brush thicknesses are 2.9 ± 0.7, 7.5 ± 0.8 and 15.9 ± 1.6 nm, respectively. For a random coil conformation, the radius of gyration (R_g) for PMMA brushes is given by $R_g = \sqrt{N/6}b$ [51], where N is the degree of polymerization and b is the monomer size ($b_{PMMA} = 0.74$ nm). Thus, R_g values for Gaussian chains are 1.6, 3.5 and 5.7 nm, respectively. For all three NPs, h is larger than R_g, suggesting that the high grafting density (0.73 chains/nm^2) produces stretched PMMA brushes. The ratio h/R_g

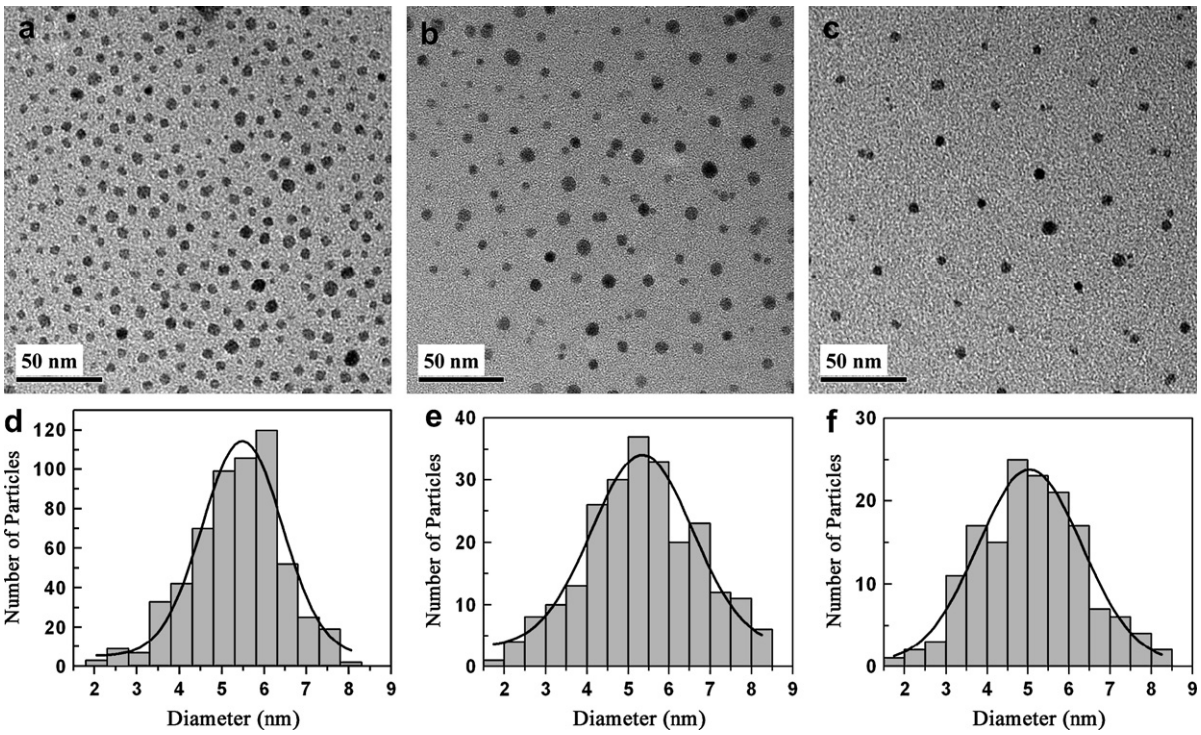

Fig. 1. TEM images of PMMA-grafted magnetite nanoparticles (a) Fe_3O_4-2.7K, (b) Fe_3O_4-13.3K and (c) Fe_3O_4-35.7K, and the corresponding histograms (d–f) of NP core diameter distribution. The average diameter for all three NPs is ~5 nm.

increases from 1.8 to 2.8 as the molecular weight of PMMA brush increases from 2.7 to 35.7 kg/mol, indicating that the polymer brush is more stretched at a higher molecular weight. Relative to a fully stretched brush ($h \sim N$), this stretching on the highly curved surface is much less because of a decrease in chain crowding near the free ends of the polymer chains.

3.2. Dispersion of NPs in homopolymer

In this section, the dispersion of PMMA-grafted magnetite NPs in PMMA-37K and PMMA-77K is discussed. At fixed grafting density (0.73 chains/nm^2), the primary factors that control dispersion of the NPs in homopolymer PMMA are the molecular weights of PMMA brushes (M) and PMMA homopolymer (P). This section shows how increasing M from 2.7 to 35.7 kg/mol affects the dispersion of NPs in matrices having $P \gg M$ to $P \sim M$. The effect of NP concentration on the dispersion of as-cast and annealed films is also explored.

3.2.1. Fe_3O_4-2.7K NP

Cross-sectional TEM images in Fig. 2 capture the dispersion of Fe_3O_4-2.7K NPs in homopolymers PMMA-37K and PMMA-77K. Fig. 2a displays the morphology of an as-cast PMMA-37K/Fe_3O_4-2.7K film containing 8 wt% NPs. The NPs are well distributed in the as-cast film and no aggregation is observed. After annealing at 185 °C for 4 days, the Fe_3O_4-2.7K NPs form aggregates in the film, as shown in Fig. 2b. The individual aggregates range in size from ~20 to ~50 nm; the average aggregate size is 30.1 ± 7.2 nm. Upon increasing the molecular weight of the matrix from 37 to 77 kg/mol, the Fe_3O_4-2.7K NPs remain uniformly dispersed in the as-cast films at 4 and 9 wt% as shown in Fig. 2c and e, respectively. Similar to the PMMA-37K case, the NPs aggregate after annealing as shown in Fig. 2d and f for films with 4 and 9 wt% NPs, respectively. The aggregate size increases from 15.1 ± 3.5 to 34.2 ± 8.1 nm as NP concentration increases from 4 to 9 wt%, respectively.

The aggregation behavior of the Fe_3O_4-2.7K NPs in PMMA is consistent with the dry brush theory [11,29]. In the dry brush regime, the molecular weight of the polymer brush is lower than that of the matrix ($M < P$) and therefore the matrix chains are unable to penetrate or wet the brush [30]. The wetting of the polymer brush by homopolymer chains of the same type depends on several parameters including the molecular weight of the brush (M), the molecular weight of the matrix chains (P), and the grafting density [30–32,47]. In general, polymer brushes with a high grafting density are not wet by a polymer matrix if $M < P$. As a result, densely grafted polymer brushes may attract each other in the presence of a chemically identical polymer melt that satisfies $P > M$ [38,47]. The aggregation or macrophase separation in the dry brush regime is also called depletion demixing [29]. For PMMA-grafted NPs in a PMMA homopolymer, there is an entropic balance between the translational entropy of the NPs and the conformational entropy of the PMMA matrix chains. When the gain in the conformational entropy of the PMMA chains is larger than the entropy loss due to aggregation of NPs, the entropic balance favors depletion demixing.

In addition to the dry brush explanation, van der Waals (VDW) and magnetic dipole–dipole interactions can introduce attraction forces that result in aggregation of PMMA-grafted Fe_3O_4 NPs. The VDW interaction energy between two spherical particles is given by [52]

$$E_{\mathrm{VDW}} = -\frac{A}{12}\left[\frac{d^2}{r^2-d^2}+\frac{d^2}{r^2}+2\ln\left(1-\frac{d^2}{r^2}\right)\right] \quad (1)$$

where A is the Hamaker constant of the NP which is about 2.1×10^{-19} J for magnetite, d is the NP diameter and r is the separation distance between NPs. For the closest center-to-center separation distance of 7 nm, the VDW interaction energy is about $0.3k_BT$ ($T = 458$ K). Because this value is smaller than the thermal fluctuation energy, the VDW interaction is not likely responsible for NP aggregation. In order to estimate the magnetic interaction, the magnetic NPs are usually taken as point dipoles with well-defined

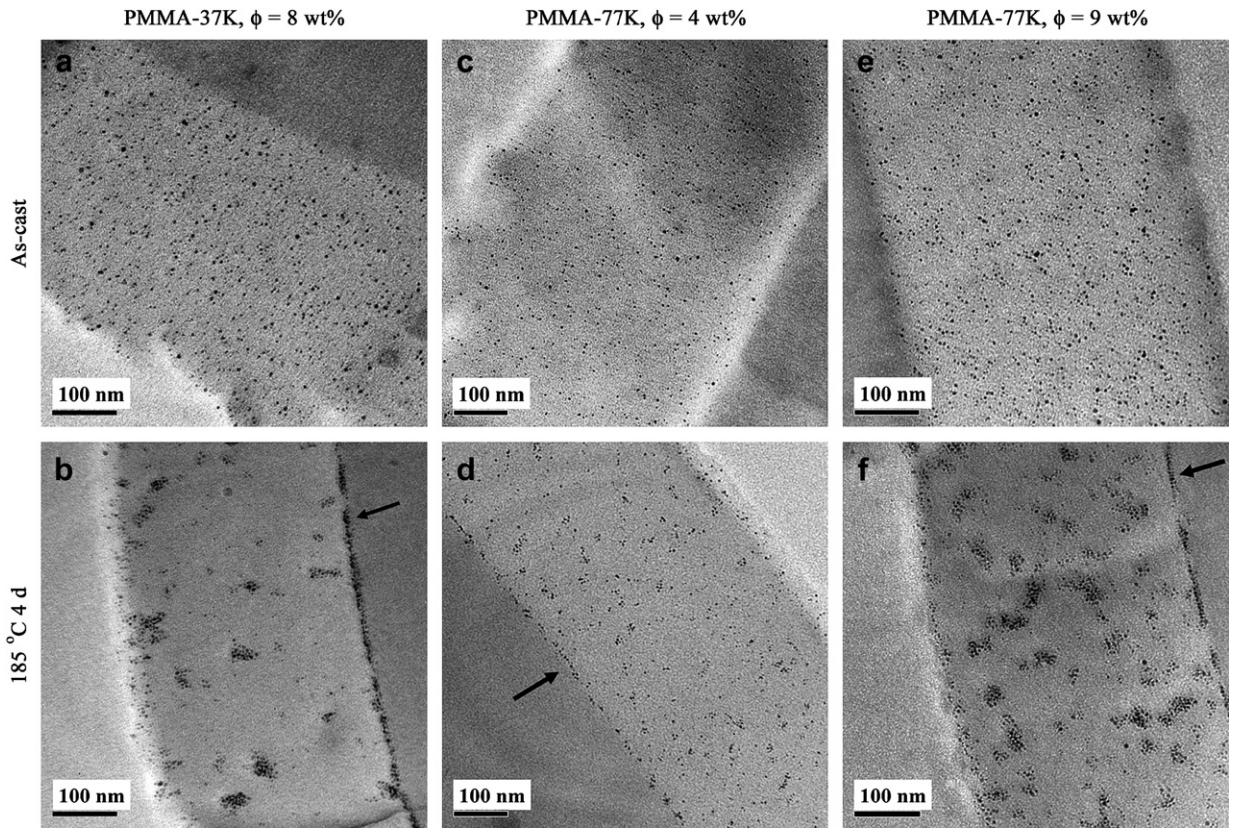

Fig. 2. Cross-sectional TEM images of nanocomposite films of PMMA-37K/Fe_3O_4-2.7K (8 wt%) before annealing (a) and after annealing at 185 °C for 4 days (b). Cross-sectional TEM images of nanocomposite films of PMMA-77K/Fe_3O_4-2.7K at two different NP concentrations: (c, d) 4 wt%, and (e, f) 9 wt%; (c, e) are the images before annealing whereas (d, f) are the images after annealing at 185 °C for 4 days. Arrows denote the film/epoxy interface, i.e., the original film surface.

magnetic moments. Assuming that the magnetic dipoles of two NPs are aligned in the same direction, the potential energy due to the magnetic dipole–dipole interaction is given by [52]

$$E_{\mathrm{dd}}(r,\theta) = \frac{\mu_0 m^2}{4\pi}\left(\frac{1-3\cos^2\theta}{r^3}\right) \quad (2)$$

where μ_0 is the magnetic constant, m is the magnetic moment, and θ is the angle between the magnetic moment and the distance vector between two NPs. The maximum potential energy is reached when the NPs are in contact with each other (i.e., $r \approx 5$ nm). The maximum energy is calculated to be 2.3×10^{-21} J ($0.4k_BT$). Thus, the magnetic dipole–dipole interaction is also too weak to cause NP aggregation. Therefore, the aggregation of Fe_3O_4-2.7K NPs in PMMA melts ($P = 37$and 77 kg/mol) likely results from the entropic cost of the long matrix chains to penetrate the short PMMA brush.

As indicated by the arrows in Fig. 2b,d and f, the Fe_3O_4-2.7K NPs also segregate to the film/air interface. Surface segregation has been reported in systems where the component with the lowest surface energy tends to segregate to the surface so that the free energy of the system is minimized. This segregation is purely driven by minimization of the enthalpic energy. However, in some cases the entropic energy is an important factor for surface or interface segregation. For example, Mackay et al. demonstrated that crosslinked polystyrene NPs in a polystyrene matrix segregated to the substrate interface [53]. Although the PS NPs lose enthalpic contacts with the polymer chains and translational entropy due to segregation, the loss is countered by the gain in the conformational entropy of the matrix PS chains via moving those chains away from the substrate. Here, surface segregation of the Fe_3O_4-2.7K NPs is driven by the conformational entropy gain of the PMMA matrix chains. The conformational entropy gain for PMMA chains of high molecular weight is larger than the translational entropy loss for the PMMA-grafted NPs with short PMMA brush. This entropic effect becomes smaller or negligible as the molecular weight of the PMMA brush increases, as discussed below for Fe_3O_4-13.3K and Fe_3O_4-35.7K.

3.2.2. Fe_3O_4-13.3K NP

The dispersion of Fe_3O_4-13.3K NPs in PMMA-37K and PMMA-77K is presented by the cross-sectional TEM images in Fig. 3. Fig. 3a shows that the Fe_3O_4-13.3K NPs at 8 wt% uniformly disperse in PMMA-37K before annealing. After annealing at 185 °C for 4 days, the NPs form aggregates in the film as shown in Fig. 3b. Interestingly, some of the NPs aggregate to form elongated shapes. Similar string-like aggregates of NPs have been reported by Lan et al. for PS-grafted silica NPs in a PS homopolymer [49]. As P increases from 37 to 77 kg/mol, the Fe_3O_4-13.3K NPs exhibit a similar behavior in the higher molecular weight matrix, i.e., uniform dispersion in the as-cast film and aggregation after annealing. Similar to blends containing the Fe_3O_4-2.7K NPs, the molecular weight of the PMMA brush on Fe_3O_4-13.3K NPs is lower than the PMMA matrices (i.e., $M < P$). Therefore, the system is in the dry brush regime, and aggregation of NPs is expected. As observed for the Fe_3O_4-2.7K case, Fe_3O_4-13.3K NPs segregate to surface. However, a comparison shows that fewer NPs are observed to segregate for the higher M brush. This result is consistent with a weaker driving force for displacing matrix chains near the surface with the Fe_3O_4-13.3K NPs, as mentioned in Section 3.2.1.

3.2.3. Fe_3O_4-35.7K NP

As discussed earlier, the dispersion of the PMMA-grafted magnetite NPs is expected to improve as the molecular weight of the brush increases. Parts a, b, c and d of Fig. 4 show the cross-sectional

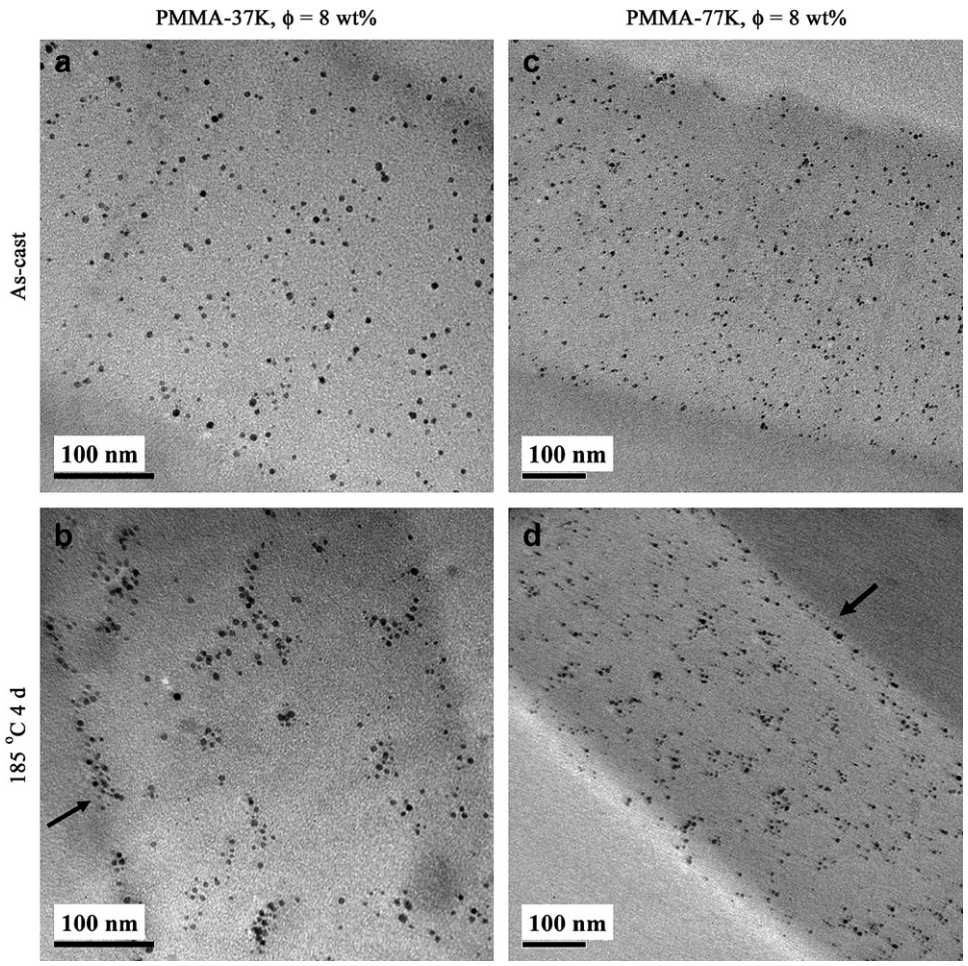

Fig. 3. Cross-sectional TEM images of nanocomposite films of PMMA-37K/Fe_3O_4-13.3K (a, b) and PMMA-77K/Fe_3O_4-13.3K (c, d). The NP concentration is 8 wt% for all images. (a, c) are the as-cast films whereas (b, d) are the films after annealing at 185 °C for 4 days. Arrows denote the original film surface.

TEM images of PMMA-37K/Fe_3O_4-35.7K films containing 8 (a and b) and 16 wt% (c and d) NPs. Note, at the same NP concentration (e.g., 8 wt%), the number density of Fe_3O_4-35.7K NPs is much less than the NPs with shorter brushes (e.g., Fe_3O_4-2.7K) because of the significant mass density difference between Fe_3O_4 and PMMA. In the as-cast films, Fig. 4a and c shows that the Fe_3O_4-35.7K NPs at 8 and 16 wt% NP, respectively, uniformly disperse in PMMA-37K. Upon annealing, the NPs do not aggregate and remain well dispersed as shown in Fig. 4b and d. This observation is consistent with wet brush theory. In the wet brush regime, the molecular weight of the matrix chains is comparable or lower than that of the polymer brush (i.e., $P < M$). As a result, the brush can be penetrated and swollen by the matrix chains, leading to a long-range repulsion between NPs. Therefore, the polymer-grafted NPs are expected to remain dispersed under wet brush conditions.

As the molecular weight of the PMMA matrix increases from 37 to 77 kg/mol (i.e., $P > M$), the dry brush conditions are satisfied and Fe_3O_4-35.7K NPs should aggregate in the PMMA-77K matrix. However, Fig. 4e and f shows that the Fe_3O_4-35.7K NPs are uniformly dispersed in PMMA-77K. A possible explanation is that although it captures the behavior of polymer grafted to planar surfaces or colloidal particles (particle diameter is much larger than brush thickness), the brush theory fails to describe the behavior of brushes attached to NPs where the core diameter is comparable or less than the brush thickness. Although there have been some studies considering the curvature effect [40], a modified brush theory taking into account NP curvature is desirable. In our paper, the grafting density of brushes is held fixed at 0.73 chains/nm^2. The curvature defined as the brush thickness divided by the core particle radius ranges from ~1 to 6 in this study. Correspondingly, the effective areal chain density at the free end of the brush decreases as M increases, resulting in a shift of the boundary between dry and wet brushes toward higher grafting density. A simple geometric calculation predicts an effective areal chain density of only ~0.01 chains/nm^2 for the Fe_3O_4-35.7K NP. Therefore, because of its high curvature, the Fe_3O_4-35.7K NPs may be wet by matrix chains with a higher molecular weight (e.g., $P = 77$ kg/mol).

3.3. Dispersion of NPs in block copolymer

In this section, the dispersion of PMMA-grafted magnetite NPs in a lamellar-forming block copolymer, PS-*b*-PMMA, is presented. The same NPs that were mixed with PMMA homopolymer (Section 3.2) are found to behave very differently in PS-*b*-PMMA. In the homopolymer case, NP dispersion is observed to improve upon increasing the molecular weight of the brush and aggregate-free nanocomposite films are obtained. However, as brush molecular weight increases, NP dispersion is reduced in the block copolymer resulting in the formation of aggregates even in the as-cast nanocomposite films. Small aggregates tend to locate at defects in the lamellae, whereas larger ones greatly perturb the morphology and become encapsulated by onion-ring copolymer structures. This aggregation is explained by a multi-component Flory–Huggins theory that predicts the phase behavior of the polymer solution prior to spin casting.

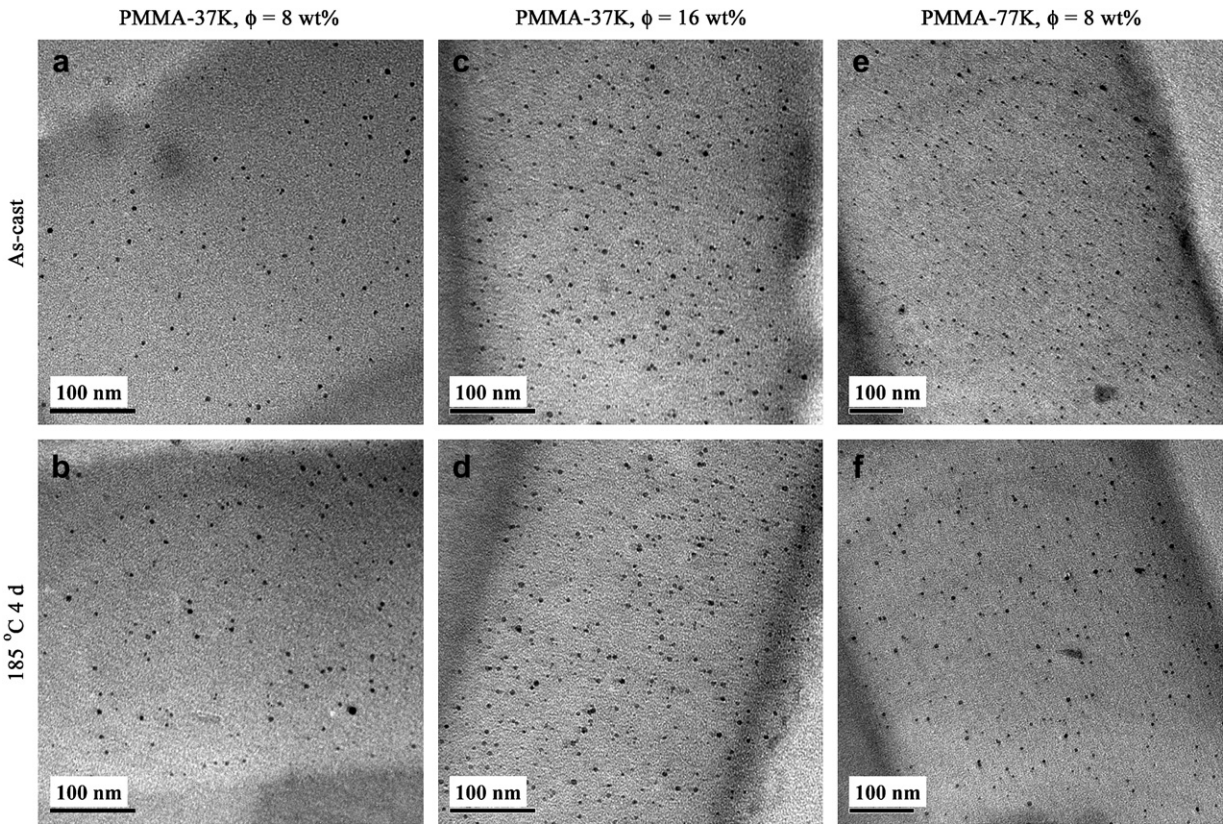

Fig. 4. Cross-sectional TEM images of nanocomposite films of PMMA-37K/Fe_3O_4-35.7K at two different NP concentrations: (a, b) 8 wt% and (c, d) 16 wt%. (a, c) are the images before annealing whereas (b, d) are the images after annealing at 185 °C for 4 days. Cross-sectional TEM images of nanocomposite films of PMMA-77K/Fe_3O_4-35.7K (8 wt%) before annealing (e) and after annealing at 185 °C for 4 days (f).

3.3.1. Fe_3O_4-2.7K NP

The dispersion of Fe_3O_4-2.7K NPs in PS-*b*-PMMA at 1 and 10 wt% is presented in Fig. 5. The AFM height image (Fig. 5a) shows the surface morphology of an as-cast PS-*b*-PMMA/Fe_3O_4-2.7K (1 wt%) film. The surface shows small, irregular, random features, but is relatively smooth with a RMS roughness of only 0.5 nm. The TEM image in Fig. 5b shows that the Fe_3O_4-2.7K NPs are uniformly dispersed in the as-cast film. Upon annealing, the PS-*b*-PMMA is expected to self-assemble into lamellae and the PMMA-grafted NPs are expected to locate within the PMMA domains. Indeed, Fig. 5c shows that the PS-*b*-PMMA forms a parallel lamellar structure with PMMA (light) and PS (dark) lamellae at the substrate and surface, respectively. Also, the Fe_3O_4-2.7K NPs have been partitioned into the PMMA domains and are uniformly distributed. Upon increasing the NP concentration to 10 wt%, Fig. 5d shows that the surface of the as-cast PS-*b*-PMMA/Fe_3O_4-2.7K film remains relatively smooth. The RMS roughness is slightly greater, 0.7 nm, than the 1 wt% case, 0.5 nm. Fig. 5e shows that the NPs are uniformly dispersed throughout the as-cast film. After annealing, the PS-*b*-PMMA is unable to self-assemble into a lamellar morphology because the Fe_3O_4-2.7K NPs have formed aggregates with an equivalent diameter of about 22 nm. For comparison, the lamellar domain size in neat PS-*b*-PMMA is about 18 nm. Similar to the PMMA/Fe_3O_4-2.7K case, the aggregation in PS-*b*-PMMA may be attributed to the inability of the long matrix block (*P*) to wet the short brush (*M*) at high grafting density (0.73 chains/nm^2), i.e., dry brush regime. The competition between the aggregation of NPs and self-assembly of the block copolymer determines the size of aggregates and the ultimate structure of nanocomposite films. For the PS-*b*-PMMA/Fe_3O_4-2.7K (10 wt%) film, aggregate formation occurs faster than PS-*b*-PMMA self-assembly. Thus, the aggregates are kinetically trapped by the encapsulating copolymer and unable to grow with further annealing. Comparison of the 1 and 10 wt% behavior suggests that the Fe_3O_4-2.7K NPs are uniformly dispersed in the PMMA lamellar domains at low NP concentration (e.g., 1 wt%) because the interparticle distance is much greater than the range of attractive forces. Calculations of the interparticle potential in a confined domain (i.e., lamellae) are needed to determine the precise mechanism responsible for aggregation of Fe_3O_4-2.7K.

3.3.2. Fe_3O_4-13.3K NP

Fig. 6 shows the dispersion of Fe_3O_4-13.3K NPs (4 wt%) in PS-*b*-PMMA. Fig. 6a shows that the surface of the as-cast film is relatively smooth, except for a few small bumps, and has a RMS roughness of 0.7 nm. As discussed below, these bumps are due to aggregates that form near the surface of the as-cast films. Fig. 6b shows the cross-sectional TEM image of the as-cast film. In contrast to Fe_3O_4-2.7K NPs in as-cast films, which uniformly disperse up to 10 wt%, the Fe_3O_4-13.3K NPs are found as both aggregates and individual NPs. Once they form in the as-cast films, the aggregates are stable throughout the annealing process and have an average size of ~37.6 nm. Fig. 6c shows the cross-sectional TEM image of PS-*b*-PMMA/Fe_3O_4-13.3K (4 wt%) after annealing at 185 °C for 10 days. Individual NPs and small NP aggregates are able to locate within PMMA domains. However, large NP aggregates are unable to fit within the PMMA domain and tend to locate at the boundary between parallel and perpendicular orientations. A detailed study of the self-assembly of block copolymer nanocomposite films will be presented in a forthcoming publication.

As discussed earlier, the dispersion of PMMA-grafted NPs in homopolymer PMMA is improved by increasing the brush molecular weight. However, in as-cast block copolymer films, an increase in the molecular weight of the brush from 2.7 to 13.3 kg/mol induces aggregation. If depletion attractive forces or entropic forces

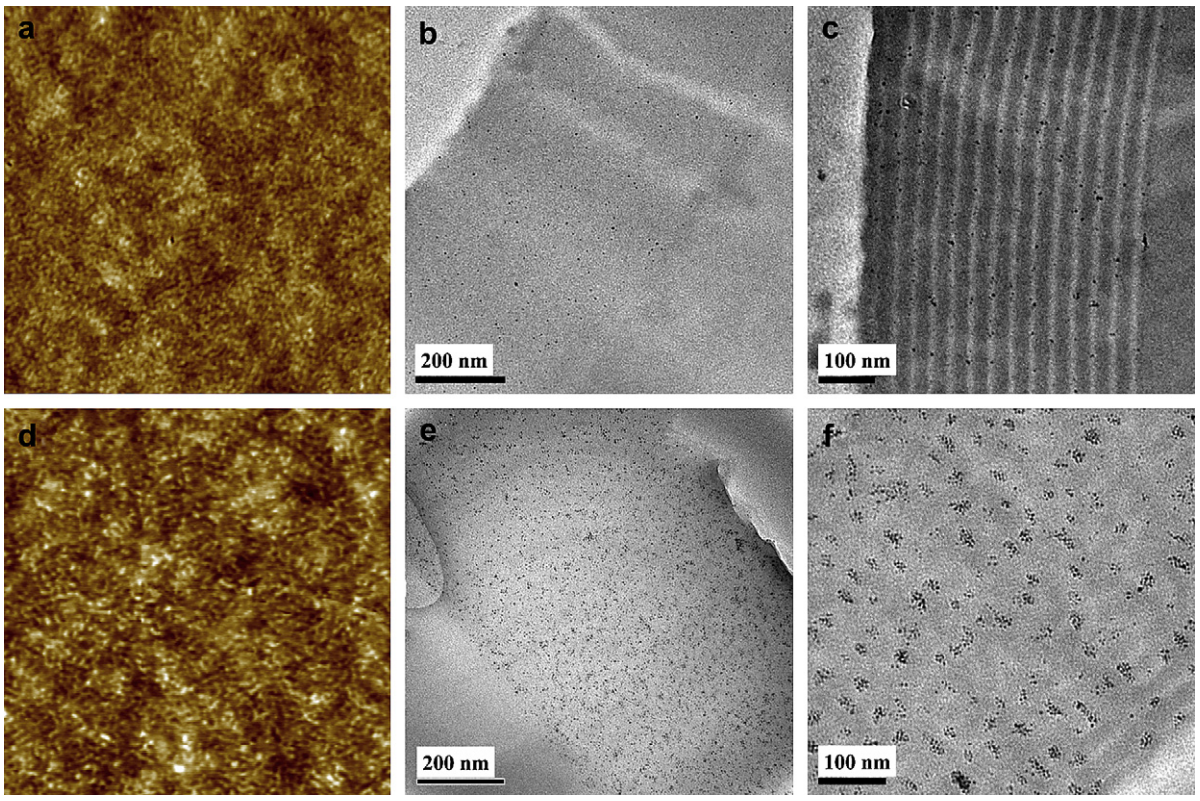

Fig. 5. (a) AFM height image and (b) cross-sectional TEM image of an as-cast PS-*b*-PMMA/Fe_3O_4-2.7K (1 wt%) film. (c) Cross-sectional TEM image of PS-*b*-PMMA/Fe_3O_4-2.7K (1 wt%) after annealing at 185 °C for 10 days. (d) AFM height image and (e) cross-sectional TEM image of an as-cast PS-*b*-PMMA/Fe_3O_4-2.7K (10 wt%) film. (f) Cross-sectional TEM image of PS-*b*-PMMA/Fe_3O_4-2.7K (10 wt%) after annealing at 185 °C for 8 days. The size of both AFM images is $2 \times 2\ \mu m^2$, and the height scale is $\Delta z = 0$–8 nm.

dominate, similar aggregation behavior would have been observed in the as-cast films of PMMA/Fe_3O_4-13.3K. We attribute aggregation in the block copolymer system to the unfavorable enthalpic interactions between PS block and PMMA brush. Namely, the Fe_3O_4-13.3K NPs have already aggregated in the block copolymer-NP-toluene solution, and remain in the dried film after spin coating. Theoretical calculations of phase stability of the polymer solutions presented in Section 3.3.4 support this argument.

3.3.3. Fe_3O_4-35.7K NP

Fig. 7 shows the dispersion of 4 and 16 wt% Fe_3O_4-35.7K NPs in PS-*b*-PMMA. Fig. 7a and d shows the surface morphology of the as-cast films at 4 and 16 wt%, respectively. The roughness increases from 0.9 to 3.6 nm as the NP concentration increases from 4 to 16 wt%. Both film surfaces contain bumps whose size increases from ~100 to ~300 nm as NP concentration increases. These bumps are consistent with the formation of NP aggregates in the near surface region of the as-cast films. Indeed, parts b and e of Fig. 7 are the corresponding cross-sectional TEM images of the as-cast films. These images show that the Fe_3O_4-35.7K NPs form aggregates with equivalent diameters of 42.7 and 164.0 nm at 4 and 16 wt% NPs, respectively. These aggregate sizes are consistent with the feature size observed on the surface by AFM. In contrast to the Fe_3O_4-13.3K NPs that exist as both aggregates and individual NPs in PS-*b*-PMMA, almost all Fe_3O_4-35.7K NPs are found in aggregates, indicating a stronger phase separation than in the Fe_3O_4-13.3K

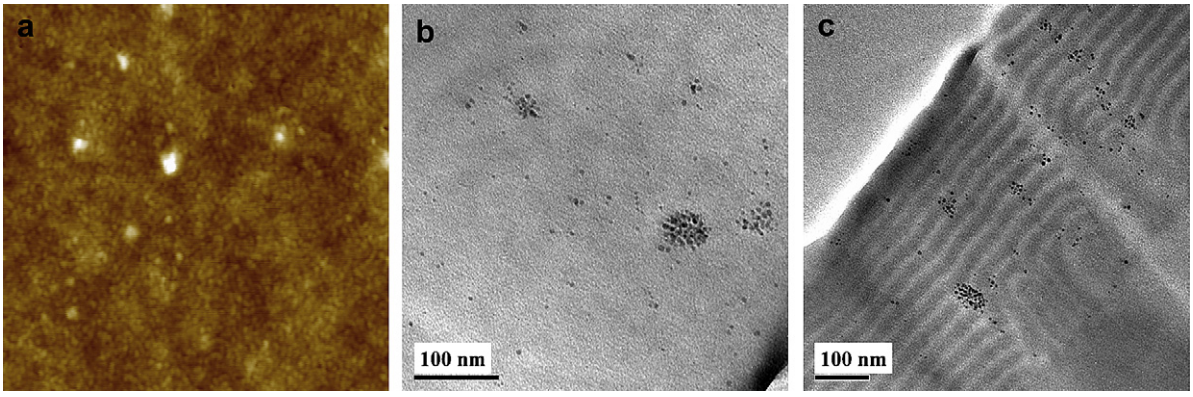

Fig. 6. (a) AFM height image and (b) cross-sectional TEM image of an as-cast PS-*b*-PMMA/Fe_3O_4-13.3K (4 wt%) film. The AFM image size is $2 \times 2\ \mu m^2$, and the height scale is $\Delta z = 0$–15 nm. (c) Cross-sectional TEM image of PS-*b*-PMMA/Fe_3O_4-13.3K (4 wt%) after annealing at 185 °C for 10 days.

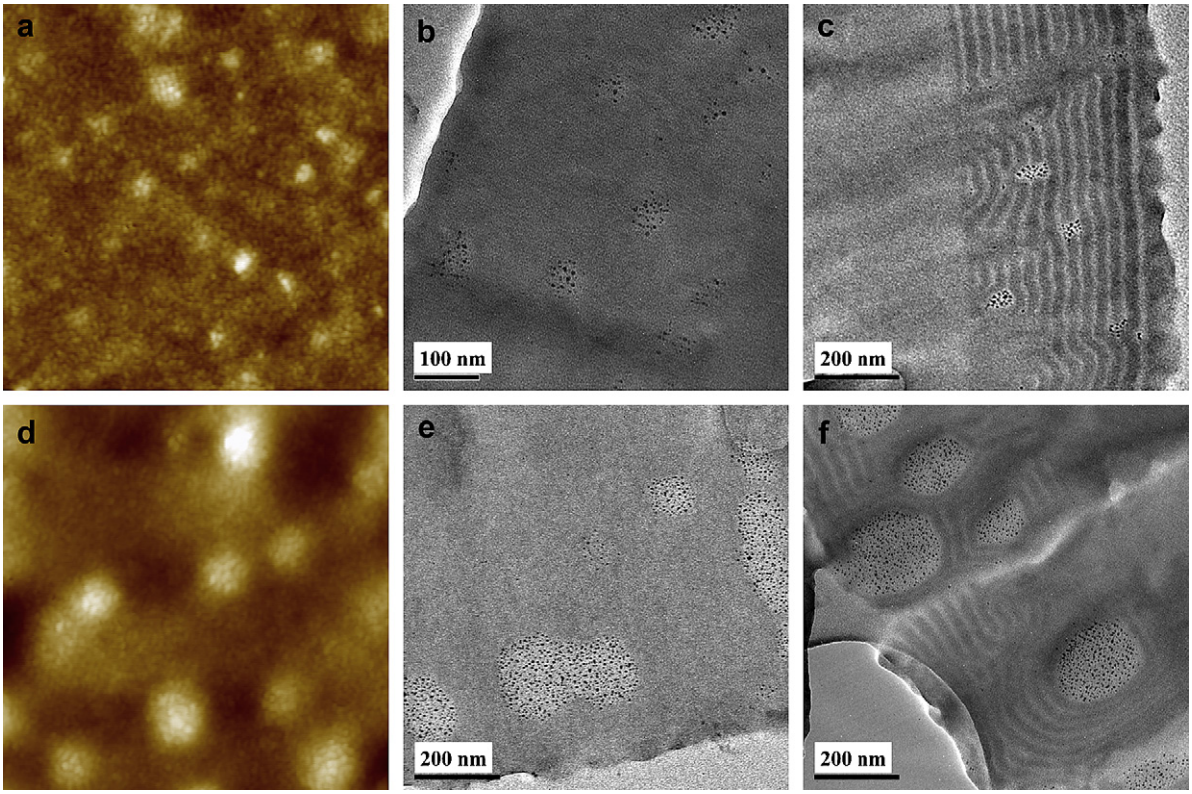

Fig. 7. (a) AFM height image and (b) cross-sectional TEM image of an as-cast PS-*b*-PMMA/Fe_3O_4-35.7K (4 wt%) film. (c) Cross-sectional TEM image of PS-*b*-PMMA/Fe_3O_4-35.7K (4 wt%) after annealing at 185 °C for 10 days. (d) AFM height image and (e) cross-sectional TEM image of an as-cast PS-*b*-PMMA/Fe_3O_4-35.7K (16 wt%) film. (f) Cross-sectional TEM image of PS-*b*-PMMA/Fe_3O_4-35.7K (16 wt%) after annealing at 185 °C for 10 days. The size of both AFM images is $2 \times 2\ \mu m^2$, and the height scale is $\Delta z = 0$–15 nm for (a) and $\Delta z = 0$–40 nm for (d).

system. Upon annealing at 185 °C, the aggregate size remains similar suggesting that the aggregates are stable upon annealing (Fig. 7c and f). The morphology of the block copolymer is greatly perturbed because the size of aggregates is greater than the lamellar period (37 nm), and as a result lamellae assemble around the aggregates (16 wt%, Fig. 7f) to form onion-ring like features.

3.3.4. Three-component Flory–Huggins model of phase stability

The aggregation of NPs grafted with long PMMA brushes in PS-*b*-PMMA may be attributed to a decrease in the compatibility between the PMMA brush and PS-*b*-PMMA as the molecular weight of the brush increases. In particular, the Fe_3O_4-13.3K and Fe_3O_4-35.7K NPs likely aggregate in the block copolymer–NP–toluene solution, and these aggregates are retained in the as-cast films. Indeed, small angle x-ray scattering measurements (not shown) indicate that Fe_3O_4-2.7K NPs are uniformly dispersed in solution containing block copolymer, whereas Fe_3O_4-13.3K and Fe_3O_4-35.7K NPs aggregate in solution. We now consider a three-component system consisting of PS-*b*-PMMA (A), PMMA-grafted NPs (B), and toluene (C). The phase behavior can be predicted by the Flory–Huggins theory, and the free energy per site is given by [54]

$$\begin{aligned} F &= \frac{f_{FH}(\phi)}{k_B T} \\ &= \frac{\phi_A}{N_A}\ln\phi_A + \frac{\phi_B}{N_B}\ln\phi_B + \frac{\phi_C}{N_C}\ln\phi_C + \chi_{AB}\phi_A\phi_B + \chi_{AC}\phi_A\phi_C \\ &\quad + \chi_{BC}\phi_B\phi_C \end{aligned} \tag{3}$$

where N_i and ϕ_i are the degree of polymerization and local composition (or volume fraction) of component *i*. Because C is a solvent, $N_C = 1$. The system is assumed to be incompressible, i.e., $\phi_A + \phi_B + \phi_C = 1$. The spinodal curves represent the limits of instability of the homogeneous phase and are determined by

$$\begin{vmatrix} \dfrac{\partial^2 F}{\partial\phi_A^2} & \dfrac{\partial^2 F}{\partial\phi_A\partial\phi_B} \\ \dfrac{\partial^2 F}{\partial\phi_B\partial\phi_A} & \dfrac{\partial^2 F}{\partial\phi_B^2} \end{vmatrix} = 0 \tag{4}$$

This equation can be rewritten as

$$\frac{\partial^2 F}{\partial\phi_A^2} \times \frac{\partial^2 F}{\partial\phi_B^2} - \left(\frac{\partial^2 F}{\partial\phi_A\partial\phi_B}\right)^2 = 0 \tag{5}$$

where the components can be solved via differentiation of Eq. (3) and are given by

$$\frac{\partial^2 F}{\partial\phi_A^2} = \frac{1}{N_A\phi_A} + \frac{1}{N_C\phi_C} - 2\chi_{AC} \tag{6}$$

$$\frac{\partial^2 F}{\partial\phi_A\partial\phi_B} = \frac{\partial^2 F}{\partial\phi_B\partial\phi_A} = \frac{1}{N_C\phi_C} + \chi_{AB} - \chi_{AC} - \chi_{BC} \tag{7}$$

$$\frac{\partial^2 F}{\partial\phi_B^2} = \frac{1}{N_B\phi_B} + \frac{1}{N_C\phi_C} - 2\chi_{BC} \tag{8}$$

Based on Eqs. (6)–(8), Eq. (5) can be derived as

$$\left(\frac{1}{N_A\phi_A}+\frac{1}{N_C\phi_C}-2\chi_{AC}\right)\times\left(\frac{1}{N_B\phi_B}+\frac{1}{N_C\phi_C}-2\chi_{BC}\right)=\left(\frac{1}{N_C\phi_C}+\chi_{AB}-\chi_{AC}-\chi_{BC}\right)^2 \quad (9)$$

To simplify the calculation, we have made a few assumptions. First, we assume that the block copolymer PS-*b*-PMMA adapts a disordered chain conformation. This assumption is reasonable because PS-*b*-PMMA is dissolved in a good solvent (toluene) for both blocks. Second, the PMMA-grafted NPs are regarded as PMMA star polymers. In Eq. (9), N_A is the degree of polymerization of PS-*b*-PMMA, whereas N_B is the total number of PMMA monomers per NP. The Flory–Huggins interaction parameters, $\chi_{PS-PMMA}$, $\chi_{PS-toluene}$ and $\chi_{PMMA-toluene}$, are taken from the literature: $\chi_{PS-PMMA}=0.04$ (at 25 °C), $\chi_{PS-toluene}=0.40$ (at 25 °C) and $\chi_{PMMA-toluene}=0.45$ (at 27 °C) [55,56]. Therefore, we could derive the effective Flory–Huggins interaction parameters in Eq. (9). Using the copolymer blend theory [57–59], χ_{AB} is determined by

$$\chi_{AB}=f_{PS}^2\chi_{PS-PMMA}=0.01 \quad (10)$$

where f_{PS} is the volume fraction of the PS block in PS-*b*-PMMA. χ_{AC} and χ_{BC} are calculated to be 0.41 and 0.45, respectively.

Because the volume fraction of PS-*b*-PMMA in solution is relatively constant, the only unknown factor in Eq. (9) is the critical volume fraction of the PMMA-grafted NPs. For ϕ_B values greater than this critical value, the PMMA-grafted NPs will macrophase separate and form aggregates in solution. The critical NP volume fractions for Fe_3O_4-2.7K, Fe_3O_4-13.3K and Fe_3O_4-35.7K are 2.0%, 0.40% and 0.16%, respectively. In our experiments, the highest concentration of Fe_3O_4-2.7K NPs is 10 wt%, which corresponds to only 0.7 vol%. Since this value is below the critical value of 2.0%, the Fe_3O_4-2.7K NPs are predicted to be stable and uniformly dispersed in solution, consistent with experimental observations. However, for the Fe_3O_4-13.3K NPs, a 4 wt% concentration corresponds to 0.63 vol%, which is slightly greater than the critical value of 0.40%. Therefore, the Fe_3O_4-13.3K NPs are predicted to form aggregates in solution, consistent with the observation of aggregate formation in as-cast films. Because 0.63 vol% is rather close to the critical concentration, individual NPs can still be observed in the as-cast films. In contrast, for the longest PMMA brush (Fe_3O_4-35.7K NPs), the corresponding volume fractions for 4 and 16 wt% NP are 1.4 and 3.3 vol%, which are much greater than the critical value of 0.16 vol%. Thus, almost all Fe_3O_4-35.7K NPs form aggregates in solution. Thus, the Flory–Huggins model accurately predicts the NP concentrations at which aggregation in nanocomposite films is expected.

4. Conclusions

Here we investigate the dispersion of PMMA-grafted magnetite NPs in homopolymer PMMA and lamellar-forming block copolymer PS-*b*-PMMA films. The NPs are grafted with PMMA brushes with molecular weights of 2.7, 13.3 and 35.7 kg/mol. The dispersion behavior of NPs in PMMA and PS-*b*-PMMA is found to be controlled by different mechanisms. For NPs with the longest PMMA brush, a uniform dispersion of NPs in PMMA is obtained, whereas decreasing the molecular weight of the brush results in NP aggregation. This behavior can be explained by wet and dry brush theory, although a more complex model taking into account the NP curvature is necessary to accurately describe systems containing polymer-grafted NPs of small diameter ($d<10$ nm). On the other hand, the dispersion of PMMA-grafted NPs in PS-*b*-PMMA is worse at high brush lengths. Namely, in as-cast films, a uniform dispersion is obtained for NPs with the shortest PMMA brush, whereas aggregation of NPs is observed as the molecular weight of brush increases. A Flory–Huggins theory describing the phase stability of the three-component solution predicts the critical concentrations at which aggregation is found in solution. These predictions are in good agreement with experimental observations.

Acknowledgement

This work was financially supported by grants from NSF/MRSEC (DMR05-20020), NSF/Polymer Program (DMR02-34903), and NSF/NSEC (DMR04-25780). We acknowledge advice from Professors Karen Winey (University of Pennsylvania) and Nigel Clarke (University of Durham). We thank Professor Grant Smith and Dr. Dmitry Bedrov (University of Utah) for helpful discussions about the interactions between polymer-grafted NPs.

References

[1] Burda C, Chen XB, Narayanan R, El Sayed MA. Chemical Reviews 2005;105(4):1025–102.
[2] Kim BJ, Bang J, Hawker CJ, Kramer EJ. Macromolecules 2006;39(12):4108–14.
[3] Kim DH, Kim SH, Lavery K, Russell TP. Nano Letters 2004;4(10):1841–4.
[4] Kim HC, Jia XQ, Stafford CM, Kim DH, McCarthy TJ, Tuominen M, et al. Advanced Materials 2001;13(11):795–7.
[5] Lazzari M, Lopez-Quintela MA. Advanced Materials 2003;15(19):1583–94.
[6] Yeh SW, Wu TL, Wei KH. Nanotechnology 2005;16(6):683–7.
[7] Ahmed SR, Kofinas P. Journal of Magnetism and Magnetic Materials 2005;288:219–23.
[8] Bockstaller MR, Mickiewicz RA, Thomas EL. Advanced Materials 2005;17(11):1331–49.
[9] Chiu JJ, Kim BJ, Kramer EJ, Pine DJ. Journal of the American Chemical Society 2005;127(14):5036–7.
[10] Corbierre MK, Cameron NS, Sutton M, Mochrie SGJ, Lurio LB, Ruhm A, et al. Journal of the American Chemical Society 2001;123(42):10411–2.
[11] Corbierre MK, Cameron NS, Sutton M, Laaziri K, Lennox RB. Langmuir 2005;21(13):6063–72.
[12] Deshmukh RD, Buxton GA, Clarke N, Composto RJ. Macromolecules 2007;40(17):6316–24.
[13] Weng CC, Wei KH. Chemistry of Materials 2003;15(15):2936–41.
[14] Mackay ME, Tuteja A, Duxbury PM, Hawker CJ, Van Horn B, Guan ZB, et al. Science 2006;311(5768):1740–3.
[15] Fogg DE, Radzilowski LH, Blanski R, Schrock RR, Thomas EL. Macromolecules 1997;30(3):417–26.
[16] Park MJ, Char K. Langmuir 2006;22(4):1375–8.
[17] El Harrak A, Carrot G, Oberdisse J, Eychenne-Baron C, Boue F. Macromolecules 2004;37(17):6376–84.
[18] Garcia I, Tercjak A, Zafeiropoulos NE, Stamm M, Mondragon I. Journal of Polymer Science, Part A: Polymer Chemistry 2007;45(20):4744–50.
[19] Garcia I, Zafeiropoulos NE, Janke A, Tercjak A, Eceiza A, Stamm M, et al. Journal of Polymer Science, Part A: Polymer Chemistry 2007;45(5):925–32.
[20] Li CZ, Benicewicz BC. Macromolecules 2005;38(14):5929–36.
[21] Li DJ, Jones GL, Dunlap JR, Hua FJ, Zhao B. Langmuir 2006;22(7):3344–51.
[22] Matsuno R, Otsuka H, Takahara A. Soft Matter 2006;2(5):415–21.
[23] Morinaga T, Ohkura M, Ohno K, Tsujii Y, Fukuda T. Macromolecules 2007;40(4):1159–64.
[24] Ohno K, Morinaga T, Koh K, Tsujii Y, Fukuda T. Macromolecules 2005;38(6):2137–42.
[25] Ranjan R, Brittain WJ. Macromolecules 2007;40(17):6217–23.
[26] Zhang MM, Liu L, Wu CL, Fu GQ, Zhao HY, He BL. Polymer 2007;48(7):1989–97.
[27] Kim BJ, Chiu JJ, Yi GR, Pine DJ, Kramer EJ. Advanced Materials 2005;17(21):2618–22.
[28] Kim BJ, Fredrickson GH, Hawker CJ, Kramer EJ. Langmuir 2007;23(14):7804–9.
[29] Borukhov I, Leibler L. Macromolecules 2002;35(13):5171–82.
[30] Gay C. Macromolecules 1997;30(19):5939–43.
[31] Hasegawa R, Aoki Y, Doi M. Macromolecules 1996;29(20):6656–62.
[32] Klos J, Pakula T. Macromolecules 2004;37(21):8145–51.
[33] Lindenblatt G, Schartl W, Pakula T, Schmidt M. Macromolecules 2000;33(25):9340–7.
[34] Lindenblatt G, Schartl W, Pakula T, Schmidt M. Macromolecules 2001;34(6):1730–6.
[35] Maas JH, Fleer GJ, Leermakers FAM, Stuart MAC. Langmuir 2002;18(23):8871–80.
[36] Martin JI, Wang ZG. Journal of Physical Chemistry 1995;99(9):2833–44.
[37] Sferrazza M, Jones RAL, Bucknall DG. Physical Review E 1999;59(4):4434–40.
[38] Xu JJ, Qiu F, Zhang HD, Yang YL. Journal of Polymer Science, Part B: Polymer Physics 2006;44(19):2811–20.
[39] Carignano MA, Szleifer I. Journal of Chemical Physics 1995;102(21):8662–9.
[40] Dan N, Tirrell M. Macromolecules 1992;25(11):2890–5.
[41] Gast AP, Leibler L. Journal of Physical Chemistry 1985;89(19):3947–9.
[42] Gast AP, Leibler L. Macromolecules 1986;19(3):686–91.
[43] Lin EK, Gast AP. Macromolecules 1996;29(1):390–7.

[44] Lindberg E, Elvingson C. Journal of Chemical Physics 2001;114(14):6343–52.
[45] Striolo A. Physical Review E 2006;74(4).
[46] Wijmans CM, Zhulina EB, Fleer GJ. Macromolecules 1994;27(12):3238–48.
[47] Yezek L, Schartl W, Chen YM, Gohr K, Schmidt M. Macromolecules 2003; 36(11):4226–35.
[48] Bates FS, Fredrickson GH. Annual Review of Physical Chemistry 1990;41: 525–57.
[49] Lan Q, Francis LF, Bates FS. Journal of Polymer Science, Part B: Polymer Physics 2007;45(16):2284–99.
[50] Sun SH, Zeng H. Journal of the American Chemical Society 2002;124(28): 8204–5.
[51] de Gennes P-G. Scaling concepts in polymer physics. Ithaca, NY: Cornell University Press; 1979.
[52] Martinez-Pedrero F, Tirado-Miranda M, Schmitt A, Callejas-Fernandez J. Colloids and Surfaces A – Physicochemical and Engineering Aspects 2005;270: 317–22.
[53] Krishnan RS, Mackay ME, Duxbury PM, Pastor A, Hawker CJ, Van Horn B, et al. Nano Letters 2007;7(2):484–9.
[54] Huang C, Delacruz MO, Swift BW. Macromolecules 1995;28(24):7996–8005.
[55] Mark JE. Physical properties of polymers handbook. New York: AIP Press; 1996.
[56] Russell TP, Hjelm RP, Seeger PA. Macromolecules 1990;23(3):890–3.
[57] Kambour RP, Bendler JT, Bopp RC. Macromolecules 1983;16(5):753–7.
[58] Paul DR, Barlow JW. Polymer 1984;25(4):487–94.
[59] Tenbrinke G, Karasz FE, Macknight WJ. Macromolecules 1983;16(12): 1827–32.